Microsc. Microanal. 18, 892–904, 2012
doi:10.1017/S1431927612001109

Microscopy AND Microanalysis

EDS Measurements of X-Ray Intensity at WDS Precision and Accuracy Using a Silicon Drift Detector

Nicholas W.M. Ritchie,* Dale E. Newbury, and Jeffrey M. Davis

Material Measurement Laboratory, National Institute of Standards and Technology, Gaithersburg, MD 20899-8372, USA

Abstract: The accuracy and precision of X-ray intensity measurements with a silicon drift detector (SDD) are compared with the same measurements performed on a wavelength dispersive spectrometer (WDS) for a variety of elements in a variety of materials. In cases of major (>0.10 mass fraction) and minor (>0.01 mass fraction) elements, the SDD is demonstrated to perform as well or better than the WDS. This is demonstrated both for simple cases in which the spectral peaks do not interfere (SRM-481, SRM-482, and SRM-479a), and for more difficult cases in which the spectral peaks have significant interferences (the Ba L/Ti K lines in a series of Ba/Ti glasses and minerals). We demonstrate that even in the case of significant interference high count SDD spectra are capable of accurately measuring Ti in glasses with Ba:Ti mass fraction ratios from 2.7:1 to 23.8:1. The results suggest that for many measurements wavelength spectrometry can be replaced with an SDD with improved accuracy and precision.

Key words: EPMA, wavelength spectrometry, silicon drift detector (SDD), energy dispersive X-ray spectrometry, electron probe microanalysis, WDS, ZAF, quantitative correction

Introduction

Lithium drifted silicon [Si(Li)] detectors were novel in 1973 when Reed and Ware published their significant article (Reed & Ware, 1973), suggesting that it was possible to perform quantitative analysis using these energy dispersive spectrometers (EDS). In their article, they identify some practical and fundamental impediments to the use of EDS detectors for quantitative analysis, but they conclude that with Si(Li) detectors "the accuracy is generally comparable with that obtained with crystal spectrometers, though the limit of detection (about 0.1%) is higher."

Many limitations discussed by Reed and Ware have been mitigated over the intervening decades. Detector electronics are much more stable. Zero offset stability has been optimized using automatic zero stabilization mechanisms. The gain stability has been improved. Today, stability of a few electron volts at Cu Kα[a] can be achieved for weeks or months in a temperature-stable laboratory. Reductions in the leakage current and electronics optimized for low noise have improved the resolution performance. Digital pulse processing has improved the X-ray throughput. Optimized fast discriminators have reduced pulse pileup. X-ray transparent windows have improved to permit viewing X-rays from elements with atomic number as small as 5. Improved algorithms for processing EDS data have allowed us to resolve difficult overlaps and to extract the most accurate peak intensities from our spectra.

[a]This article uses IUPAC (Jenkins et al., 1991) notation to identify individual transitions and Siegbahn notation to refer to line families, such as the K-L_2 and K-L_3, which make up the Cu Kα peak.

Received July 18, 2011; accepted April 15, 2012
*Corresponding author. E-mail: nicholas.ritchie@nist.gov

Despite the initial promise and this technical progress, EDS detectors are still viewed as inferior to wavelength dispersive spectrometers (WDS) for quantitative work. The most common reasons quoted for the inferiority of EDS detectors are the poor peak-to-background ratios, and the inability to resolve fully most X-ray peak interferences.

Of all the improvements in energy dispersive spectrometry, arguably the most significant is the introduction of the silicon drift detector (SDD) (Gatti & Rehak, 1984; Fiorini et al., 1997). The SDD represents a radical rethinking of the collection of electron-hole pairs generated when an energetic X-ray is absorbed by a biased block of silicon. A Si(Li) detector is constructed like a capacitor with an anode and cathode on opposing faces of the detector. The capacitor creates a simple transverse field. The electrons are drawn to the anode by a bias voltage, and the size of the charge pulse is measured using charge-sensitive electronics. In an SDD, the electron holes are generated in an identical manner, but the electrons are channeled by radial and transverse-shaped electric fields to an anode where they are measured. The most significant difference between the Si(Li) and SDD designs is the size of the charge collection anode. On a Si(Li) detector, the area of the anode is equal to the active area of the detector, which is typically on the order of 10 mm^2. On an SDD, the area of the anode is independent of the active area of the detector and is typically 1,000 to 10,000 times smaller. Since the capacitance of a parallel plate capacitor is proportional to the area and inversely proportional to the spacing, the capacitance of the SDD anode is many orders of magnitude smaller than the capacitance of a Si(Li) anode. The lower capacitance allows the SDD to respond much more quickly to an electron pulse and for the charge-sensitive amplifier to amplify the signal with lower electronic noise. Shorter

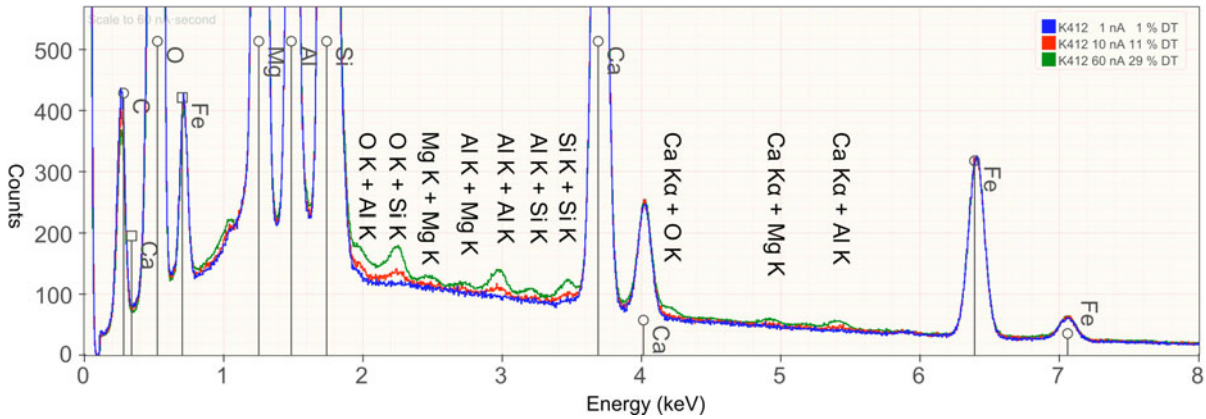

Figure 1. K412 spectra collected at 15 keV over a range of probe currents. As the probe current increases, the dead time increases and coincidence peaks start to grow at the energies representing sums of characteristic line energies. 1 nA has the smallest artifacts, and each increase in probe current increases the size of the artifacts. The major coincidences have been labeled with the most significant source lines.

duration electron pulses can be translated into greater X-ray throughput.

A consequence of these design differences is that, whereas Si(Li) detector throughput plateaus at around 5,000 cps at best resolution [~132 eV full-width at half-maximum (FWHM)], the best SDD detectors are capable of at least ten times the throughput at better resolution (~125 eV FWHM). The SDD throughput is sufficient under routine conditions to produce spectral integrals (0.1 keV to E_0) of 10 million counts in 100 s of live time.

Throughput is beneficial for accurate quantification, but it is not sufficient. Other characteristics, such as linearity of output count rate with dose, gain stability, and resolution stability, are also important. Many early adopters of SDD in microanalysis emphasized greatly increased throughput for crude quantitative work such as X-ray spectrum imaging. For this application, in many cases, these shortcomings could be overlooked. Accurate quantitative work requires more care. Coincidence events are particularly troublesome (see Fig. 1). A coincidence event, also known as pulse pile-up, occurs when the charge pulse from two or more X-rays reaches the anode sufficiently close in time that the electronics cannot distinguish the resulting pulse from a single X-ray with an energy equal to the sum of the incident X-ray energies. Discernible coincidence peaks first appear at twice the energy of the most intense characteristic peak. They can also occur at the sum energy of any pair of characteristic peaks. More insidious are the coincidence events that result from continuum X-rays with characteristic peaks or other continuum X-rays as these can occur at any energy and cannot be discerned as discrete peaks. Coincidence events can also create counts at energies above the Duane-Hunt limit. These events make estimating the true Duane-Hunt limit more challenging.

The best way to handle near simultaneous X-ray events is in the pulse processing electronics. The fast discriminator and other pulse processing logic are designed to be able to discern coincidence events by looking at the separation of pulse charge integrator steps, changes in the slope of the steps, and other subtle effects. The pulse-pair resolving time is a measure of the electronics' ability to distinguish sequential events and is a function of the X-ray energies. Resolving times are typically on the order of tens to hundreds of nanoseconds. When a coincidence event is detected, the event is discarded, and the live time is adjusted to compensate.

Another good way to eliminate coincidence events is to reduce the input count rate. At low input count rates, coincidence events are rare, but as the input count rate increases they become more common. Coincidence events affect both Si(Li) detectors and SDDs. The old rule of thumb for Si(Li) detectors was to aim for a dead time of approximately 30% to 50%. The situation is less clear-cut for SDD. Dead time is a function of the time to process each pulse while pulse-pair rejection is a function of an independent circuit, the fast discriminator. At the faster rates typical of an SDD, the fast discriminator may not be able to handle 30% dead time at the short pulse processing times. In our experience, with various vendor's SDD, it is necessary to determine the appropriate dead time for each detector and time constant.

Coincidence events are damaging to quantitative analysis. Each coincidence event corresponds to the loss of two (or more) X-rays from their appropriate energies. If the standard and unknown are measured at similar coincidence rates, coincidences in the standard compensates for coincidences in the unknown. Regardless, for 0.001 mass fraction accuracy, it is appropriate to aim for less than a 0.001 coincidence fraction. With our Bruker 4040 detector (Bruker, Karlsruhe, Germany) at the medium time constant (130 kcps setting), dead times of 10% or less produce sufficiently small numbers of coincidence events as is appropriate for quantitative work with major or minor elements. For trace element analysis, it may be necessary to further reduce the

dead time if a coincidence peak falls near a characteristic energy associated with a trace element.

Another way to deal with coincidence events is to post-process the raw spectrum data to reassign coincidence events back to the pair of energies from which they came (Statham, 1977). This algorithm requires a thorough understanding of the pulse-pair resolving characteristics of the detector system for all possible pairs of X-ray energies. With this information, it is possible to not only correct characteristic peak coincidences, but also to correct for coincidences involving continuum X-rays.

Finally, collecting standards and unknowns of similar composition under similar experimental conditions also helps to compensate for coincidence events.

This article reevaluates the claim of Reed and Ware (1973) using a modern, high-performance array of four matched SDDs capable of a combined throughput of 100,000 cps at a dead time of approximately 10% with excellent peak channel and peak width stability over the full output range. To permit a rigorous comparison, SDD measurements are made at the same time as WDS measurements as this eliminates many sources of variance, such as beam stability and sample inhomogeneity.

Materials and Methods

To properly compare SDD and WDS X-ray intensity measurements, the measurement protocol for quantitative electron-excited X-ray microanalysis with WDS introduced by Castaing (1951) was followed. To overcome the complexities of the varying WDS efficiency as a function of photon energy, Castaing introduced the concept of the *k*-ratio, the ratio of the intensities for a specific characteristic X-ray peak measured sequentially under exactly the same conditions in the unknown and a standard (a pure element or a microscopically homogeneous mixture of elements of known concentrations):

$$k = \frac{I_{unk}}{I_{std}}, \tag{1}$$

By forming this ratio of measured X-ray intensities, the detection efficiency cancels quantitatively. The same is true for the *k*-ratio measured with an SDD. The *k*-ratio depends only upon the compositional differences between the unknown and standard(s), and is independent of the type of spectrometer used for the measurement. Determining the concentration values from the set of *k*-ratios requires the calculation of "matrix corrections," which compensate for differences in the electron interactions and generation and propagation of X-rays between the unknown and standard(s). We avoid the additional complexity and uncertainty introduced by a full quantitative correction procedure by comparing the WDS and SDD *k*-ratios directly.

Equation (1) while essentially correct is not strictly an accurate representation of how we actually perform the measurement. I is not measured directly. Instead, we count the X-rays collected by a detector with a certain geometric and quantum efficiency. A more complete description would include terms Ω and ϵ to account for the geometric and quantum efficiency of the detector.

$$k = \frac{I_{unk}[\Omega\epsilon]_{unk}}{I_{std}[\Omega\epsilon]_{std}}. \tag{2}$$

This parametrization of the detector function is somewhat arbitrary but dividing it into two terms Ω and ϵ is convenient. Ω is defined to depend only on geometry—the position of the sample, the position of the detector, and the acceptance angle of the detector. Ω is independent of X-ray energy. ϵ depends upon the characteristics of the detector, the diffracting crystal (for WDS), windows, and coatings, and has a dependence on X-ray energy. For both WDS and EDS, we strive to measure the sample and unknown at the same spectrometer position and at the same X-ray energy, $[\Omega \cdot \epsilon]_{unk} = [\Omega \cdot \epsilon]_{std}$, and equation (2) reduces to equation (1).

Ω and ϵ are very different for WDS and SDD, but this difference can be ignored, except inasmuch as the product influences the magnitude of the measured signal and thus also the variance of the signal. In terms of X-ray counts per unit time per unit of beam current, an SDD typically exceeds a WDS—often by a factor of 10 or more.

The measurements were performed on JEOL JXA-8500F (JEOL Ltd., Tokyo, Japan) a Schottky field-emission electron microprobe with three wavelength spectrometers, and a four SDD cluster.[b] The JXA-8500F is equipped with a four crystal turret with LDE2, LDE1, PETJ, and TAPJ crystals on spectrometer 1, and a two crystal turret with PETJ and LIF crystals on each of spectrometers 2 and 3. The SDD is a Bruker 4040 with four 10 mm^2 active elements mounted in a single snout. Each detector is associated with an independent pulse processor. The spectra from each of the four pulse processors are accessible individually through Bruker's Quantax software, or the sum of all four is available as a single spectrum. At best resolution, the 4040 is capable of 124.3 eV at Mn Kα. A moderate throughput (the 130 kcps setting) with a compromised resolution of about 128 eV at Mn Kα was selected. The wavelength and drift detectors are mounted at a take off angle of 40°. The SDD is mounted at a distance of approximately 72 mm from the sample, providing a solid angle of $\Omega = 0.0077$ sR.

The SDD measurements were performed at a dead time of approximately 10%. This dead time was chosen to minimize the influence of coincidence events. In our experience with the 4040, dead times of 20% or higher produce an unacceptable coincidence event rate. Operating at 10% dead time represents a conservative counting strategy. At 15 or 20 keV, a 5 nA probe current produces approximately a 10% dead time.

[b] Any mention of commercial products is for information only; it does not imply recommendation or endorsement by the National Institute of Standards and Technology (NIST) nor does it imply that the products mentioned are necessarily the best available for the purpose.

The WDS and SDD measurements were performed simultaneously, whenever possible, using Probe Software's Probe for EPMA (PfE) software to control both the JEOL microprobe and Bruker SDD. Spectra were archived in the PfE analysis database, and exported in EMSA format (Egerton et al., 1991). Since both SDD and WDS data were collected simultaneously, it was necessary to choose a probe current compatible with both kinds of detectors. The SDD throughput was the limiting factor since $[\Omega \cdot \epsilon]_{SDD} > [\Omega \cdot \epsilon]_{WDS}$. The probe was defocused to 5 μm to mitigate sample damage, contamination, and localized sample inhomogeneity.

Judicious choices of high and low background wavelengths are critical for accurate *k*-ratio measurements using WDS. Wavelength scans were performed on each unknown to determine the position of interferences and to select the optimal background locations.

Similar acquisition durations were used for both the WDS and SDD data. For most analyses, this meant an SDD acquisition time of 60 s and a WDS acquisition time of 40 s/10 s/10 s (on-peak/low/high). In a certain sense, this could be argued to represent a fair comparison, but in another sense it could be argued that it does not account for all the time spent configuring, peaking, and tuning the wavelength spectrometers, performing wavelength scans to select low and high background points, and the time spent moving the spectrometers. (Some of these steps can be skipped for the special case of analyzing a sample for which a protocol has already been established.) Furthermore, since our JEOL 8500F has three wavelength spectrometers, analyses with more than three elements require multiple measurements per spectrometer with the associated move and collection time. In our experience, configuring a WDS acquisition takes many times longer than configuring an SDD acquisition. The closest equivalent for the SDD is our local practice of collecting a single Cu spectrum at the beginning of each measurement campaign. We use this spectrum to verify and track the performance and calibration of the SDD detector. Fortunately, after the combined WDS-SDD analysis protocol has been defined, it can be executed under automation—a process that often takes hours to complete. Automation is a practical necessity for WDS, but is also extremely beneficial when using the SDD for high-precision quantification.

Realistic uncertainty estimates on the measurements are desirable to permit statistically meaningful comparisons. Ultimately, both WDS and SDD are limited by Poisson (counting) statistics. In WDS, the statistics are determined by the number of counts in the peak, and high and low energy backgrounds. With EDS spectra, typically one uses weighted, linear least-squares fitting to fit an unknown spectrum peak with a standard (reference) peak to determine the *k*-ratio. The uncertainty due to Poisson statistics is ascertained from the covariance matrix. However, in any realistic measurement, there are other factors that contribute to the measurement uncertainty, such as sample inhomogeneity and instrumental drift. To determine the true variance, we made eight measurements on each sample, and reported the average and the standard deviation of the *k*-ratios.

Table 1. The Certified Composition (Mass Fraction) of NIST SRM-481 (Gold-Silver) and SRM-482 (Gold-Copper) Alloys for Microanalysis.

SRM-481	Au	Ag	SRM-482	Au	Cu
Au	1.0000	0.0000	Au	1.0000	0.0000
Au80-Ag20	0.8005	0.1996	Au80-Cu20	0.8015	0.1983
Au60-Ag40	0.6005	0.3992	Au60-Cu40	0.6036	0.3964
Au40-Ag60	0.4003	0.5993	Au40-Cu60	0.4010	0.5992
Au20-Ag80	0.2243	0.7758	Au20-Cu80	0.2012	0.7985
Ag	0.0000	1.0000	Cu	0.0000	1.0000

Table 2. The Composition (Mass Fraction) of the 9 Ba-Ti Bearing Minerals, Compounds, and Glasses.

Material	Si	Ti	O	Ba
$BaTiO_3$	0.0000	0.2053	0.2058	0.5889
K2536	0.1169	0.1619	0.2913	0.4299
K2538	0.1402	0.1319	0.2980	0.4299
K2469	0.1683	0.0959	0.3059	0.4299
K2468	0.1870	0.0719	0.3112	0.4299
K2467	0.1982	0.0576	0.3143	0.4299
Benitoite	0.2038	0.1158	0.3483	0.3322
K2466	0.2057	0.0480	0.3164	0.4299
K2496	0.2291	0.0180	0.3230	0.4299

SDD spectra were processed using NIST DTSA-II X-ray spectrum processing software (Deneb release) (Ritchie, 2011). Spectra were fit using a top-hat filter (Schamber, 1977) to account for bremsstrahlung, and a multiple-linear least-squares algorithm using singular value decomposition to fit reference spectra to standard and unknown spectra. Quantitative corrections, when performed, used the XPP algorithm (Pouchou & Pichoir, 1991) with FFAST mass absorption coefficients (Chantler et al., 2005).

Materials

Several materials were chosen to investigate both major element analysis without interferences, and some interesting peak interference and absorption edge cases. For an example of a routine analysis of materials with only major constituents (>0.10 mass fraction) and no overlaps, the NIST SRM-481 (gold-silver) and SRM-482 (gold-copper) alloys (Meinke, 1969*a*, 1969*b*) (see Table 1) were selected. For a slightly more complex situation in which a Kα X-ray overlaps a Kβ X-ray, NIST SRM-479a (Marinenko et al., 1981) was selected. SRM-479a has a certified composition of Fe 0.710 mass fraction, Cr 0.183 mass fraction, and Ni 0.107 mass fraction. For an even more complex series of overlaps, a range of Ba-Ti bearing minerals and glasses (see Table 2) with Ba/Ti mass fraction ratios varying from 2.7 to 23.8 were selected. The Ba L_3-M_5 and the Ti K-L_3 differ in energy by 45 eV (Chantler et al., 2005), as shown in Figure 2.

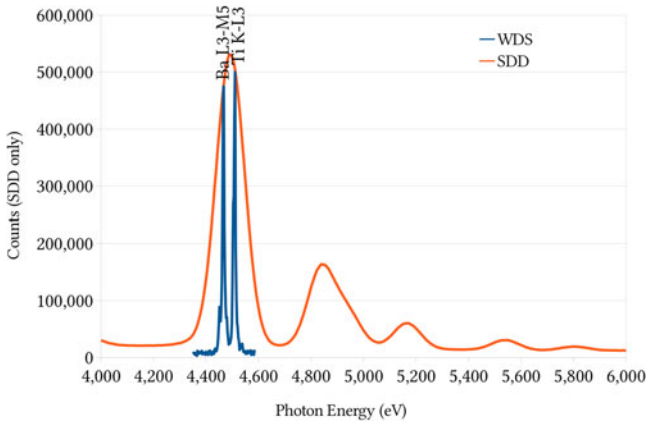

Figure 2. The Ba L and Ti K lines in benitoite. The red curve is a spectrum collected with an SDD, and the blue curve is a wavelength scan over the Ba L3-M5 and Ti K-L3 transition collected with a LiF WDS.

Results

SRM-470a

The experimental configuration for measuring SRM-479a is summarized in Table 3. The data were collected at 15 keV. EDS and WDS data were collected at 12 nA (low current), and WDS only data were collected at 100 nA (high current). In addition to Fe, Cr, and Ni, which we knew to be present in the alloy, the Si K line was also measured. Si is a difficult element to perform trace element analysis using a Si-based detector because of the presence of the Si absorption edge and internal fluorescence peak, which mimic a small Si peak.

The results, presented in Figure 3, show that the agreement between the average high current WDS measurements and the average SDD measurements is very good for the major constituents of SRM-479a. The average SDD measurement deviates by −0.5%, 0.4%,−0.2% (relative) for the Fe Kα, Ni Kα, and Cr K measurements, respectively. Examining the Fe Kα measurement, we see that the variance of the SDD measurements suggests a very slight systematic underestimation of the k-ratio as determined by WDS. The best estimate of the actual k-ratio is 0.6950 ± 0.0013 (1σ) from WDS compared to 0.6915 ± 0.0004 (1σ) for the SDD. The difference between WDS and SDD k-ratio, 0.0035, represents 2.6σ. Notice that the actual measured variability is lower for the SDD than for the WDS, even when the WDS data were collected with a high probe current and an equivalent duration.

The best estimate of the Ni Kα k-ratio was 0.0987 ± 0.0006 (1σ) for WDS and 0.0991 ± 0.0002 (1σ) for SDD. The SDD measurement fell within 1σ of the WDS measurement. The best estimate for the Cr K k-ratio was 0.2174 ± 0.0004 for WDS and 0.2169 ± 0.0001 for the SDD. The difference represents approximately 1σ.

The best estimate for the Si K k-ratio was −0.0002 ± 0.0000 for WDS and 0.0008 ± 0.0000 for SDD. Assuming a true value of 0.0000 for the Si K k-ratio, the SDD measurement was approximately 20σ too high.

For SRM-479a, the SDD was essentially able to replicate the high current WDS data with an extraordinary degree of precision for the three elements that were present. Si exposes a shortcoming of the filter-fit technique. Since the background is filtered not modeled, the algorithm has difficulty differentiating between a Si edge/internal fluorescence peak and a Si peak. The spectrum deconvolution algorithm incorrectly interpreted the Si absorption edge structure/internal fluorescence peak, which represent artifacts present in all Si(Li) and SDD detectors as a trace level of Si. The SDD could perform much better at this particular measurement if the background was measured or modeled to handle the Si edge.

SRM-481 and SRM-482

The experimental configuration for the SRM-481/482 measurement is summarized in Table 4. The data were collected at 20 keV with a 7.5 nA probe of 5 μm diameter. The results are summarized in Figures 4 and 5. Figure 4 compares the k-ratios collected via SDD and WDS side-by-side. Figure 5 examines the difference between the SDD k-ratio and the WDS k-ratio, and how this compares with the variance of the measurement.

The results for SRM-481 and SRM-482 (Figs. 4, 5) typically show very good agreement between the WDS and SDD k-ratio measurements over the full range of Au-Cu and Au-Ag alloys. Consider the Au L results in Figure 5A. Six of the eight measurements are within 1σ. The other two

Table 3. The Experimental Conditions under Which the SRM-479a Data Were Collected.*

JXA-8500F—15 keV, 12 nA and 100 nA, 5 μm Probe								
Element	Line	Crystal	On (s)	High (s)	Low (s)	On (mm)	High (mm)	Low (mm)
Cr	K-L3	LiF	40	10	10	159.28	161.13	157.53
Fe	K-L3	LiF	40	10	10	134.33	135.78	132.79
Si	K-L3	TAPJ	40	10	10	76.92	81.45	72.38
Ni	K-L3	LiF	40	10	10	115.33	117.67	113.4

*The spectrometer positions are reported in terms of the L-value, which is related to the wavelength λ by the relation $\lambda = (d/R)L$, where d is the crystal plane spacing and R is the radius of the Roland circle. EDS live time: 60 s, ~90 kcps, 8% dead time.

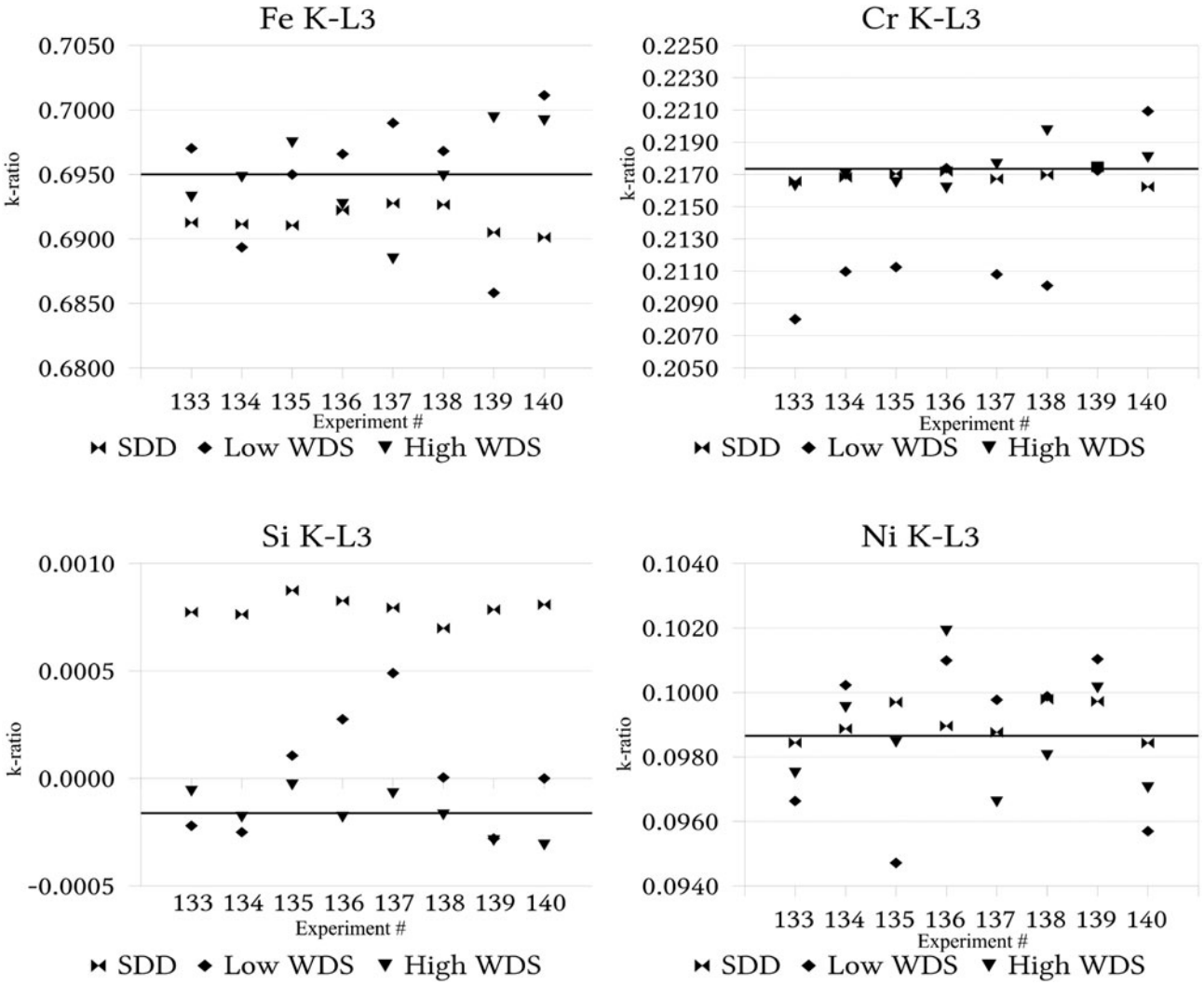

Figure 3. Comparing the *k*-ratios measured on SRM-479a (Marinenko et al., 1981) using the SDD, WDS at 12 nA (low WDS), and WDS at 100 nA (high WDS).

measurements have significant deviations of 7σ and 5σ. For Au M, all eight measurements fall within 2.65σ, with half falling within 1.1σ. For Ag L, all fall within 2σ, and six fall within 1σ, even though the later four represent measurements of no Ag (Au-Cu alloy). This is interesting to contrast with the case of Si in SRM-479a. In this case, the measurement of zero was more reliable because there is no equivalent artifact to the Si K edge near the Ag L line. For Cu Kα, six of the measurements are within 1.2σ, one is 2.3σ, and one is 9.4σ. The Cu60/Au40 measurement at 9.4σ is hard

Table 4. The Experimental Conditions under Which the SRM-481 and SRM-482 Data Were Collected.*

JXA-8500F—20 keV, 7.5 nA, 5 μm Probe									
Element	Standard	Line	Crystal	On (s)	High (s)	Low (s)	On Peak (mm)	High (mm)	Low (mm)
Au	Au	M5-N7	TAPJ	40	10	10	63.65	74.19	63.2
Au	Au	L3-M5	LiF	40	10	10	89.23	91.25	86.41
Au	Au	M5-N7	PETJ	40	10	10	187.26	189.32	184.66
Ag	Ag	L3-M5	PETJ	40	10	10	132.93	135.37	130.53
Cu	Cu	K-L3	LiF	40	10	10	107.56	109.31	105.41
Cu	Cu	L3-M5	TAPJ	40	10	10	145.22	148.58	139.34

*The measurements highlighted in gray are reported. OCR is the total output count rate for all four detectors. EDS: 180 s live time, ~10% dead time, 130 kcps OCR.

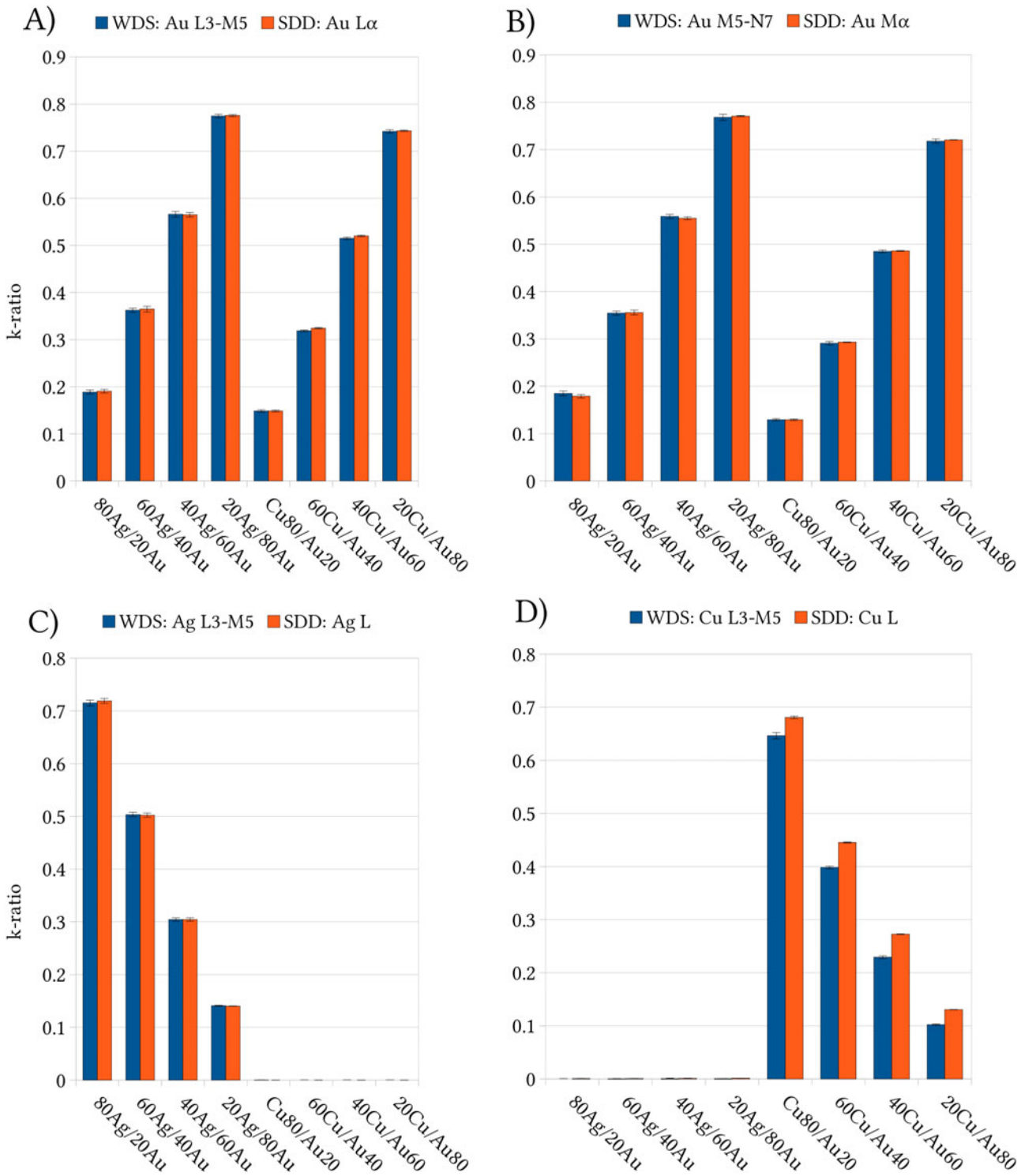

Figure 4. Compares the *k*-ratio measured by WDS with the *k*-ratio measured by SDD. The agreement is very good for the Au L and M, Ag L and Cu K lines but poorer for the Cu L. We explain the poor results for Cu L as due as differential self-absorption of the Cu L3-M5 and the Cu L2-M4.

to explain. The Cu60/Au40 measurements were consistently among the poorest, but this one is significantly worse than the rest.

The Cu L in Figures 4D and 5E represents the most interesting case and took a special effort to understand. The measurements of Cu in the Au-Ag alloys were consistent with zero with less precision than the measurements of Ag in the Au-Cu alloys. Regardless, all the *k*-ratios were less than 0.1%. The Cu L *k*-ratios in the Au-Cu alloys do not agree well. The SDD *k*-ratios are consistently larger then the WDS *k*-ratios by 5.1%, 10.6%, 15.8%, and 21.8% for 80Cu/Au20, 60Cu/Au40, 40Cu/Au60, and 20Cu/Au80.

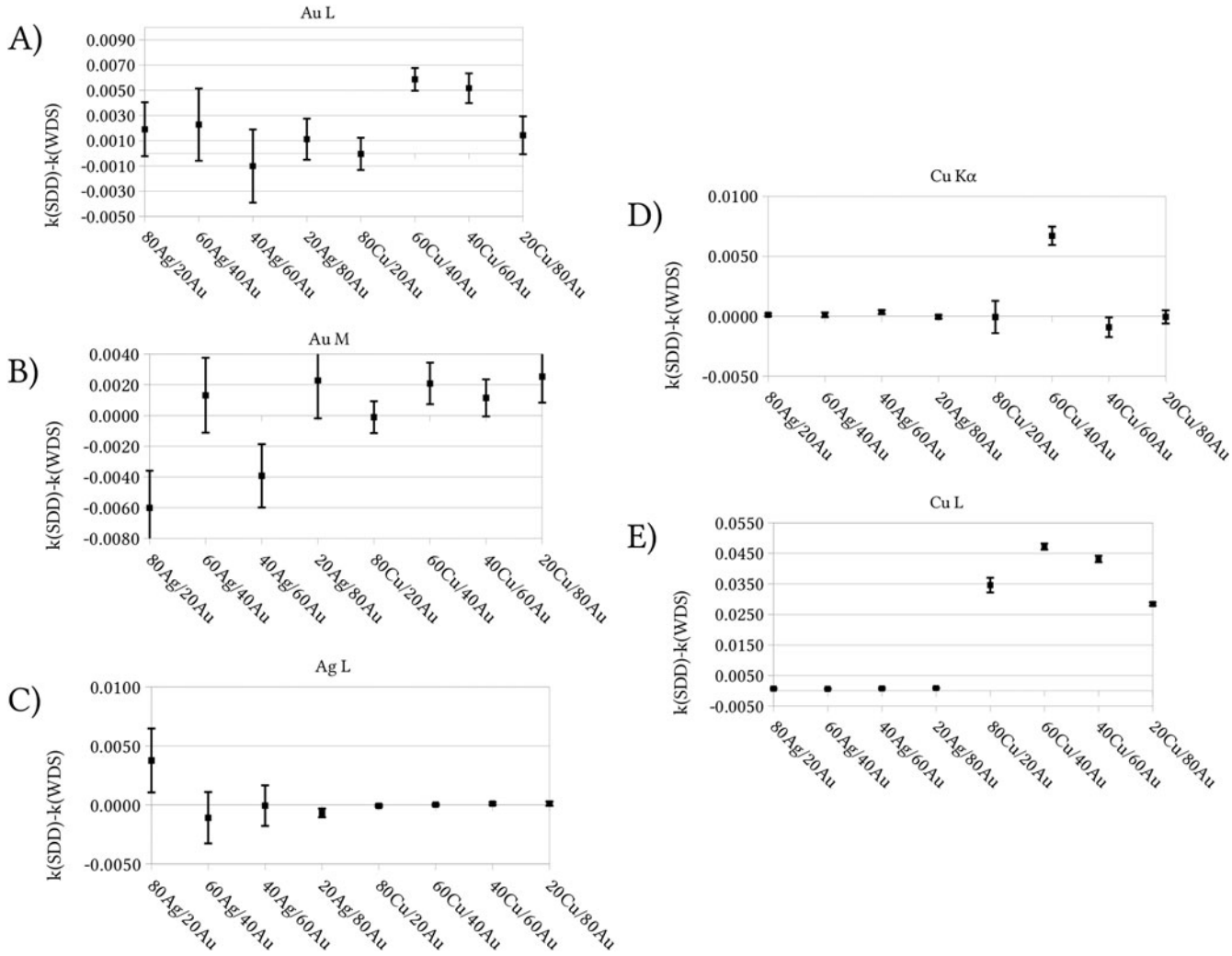

Figure 5. A careful examination of the accuracy and precision with which the SDD data match the WDS data for SRM-481 and SRM-482 (Meinke, 1969*a*, 1969*b*).

Several possible explanations were considered. (1) Initially, we suspected measurement error. The WDS measurements were repeated taking particular care to select the low and high backgrounds using fresh wavelength scans. The results were substantively the same. (2) We considered that these measurements might represent an anomaly with the particular model of SDD, so we repeated the measurement on an ASPEX Personal scanning electron microscope (SEM) (ASPEX Corporation, Delmont, PA, USA) with an e2v SDD detector, and on a FEI DualBeam focused ion beam (FEI Company, Hillsboro, OR, USA) with an Oxford INCA 80 mm^2 SDD detector (Oxford Instruments, Abingdon, Oxfordshire, UK). The results were essentially equivalent to the original measurements. (3) We considered that the results might be an artifact of the filter-fitting technique used by DTSA-II. Performing the peak integration using a modeled background did not substantially change the results. (4) We considered that the deviation might result from a nonlinearity with output count rate with respect to probe current. Measurements at 0.518, 0.995, 2.00, and 4.00 nA were not substantially different from those made at 10.0 nA. (5) Finally, we considered that the difference might represent a fundamental difference between the SDD and WDS measurements—the WDS measurement represents the measurement of a single characteristic line (the Cu L_3-M_5) and the SDD measurement represents the measurement of the whole Cu L family of lines.

This consideration turned out to be key to understanding the disparity. The crux is shown in Figure 6, a wavelength scan over the Cu L_2-M_4 and Cu L_3-M_5 lines. The plot is scaled to equalize the intensity in the Cu L_3-M_5. The intensity in the Cu L_2-M_4 varies with Cu concentration, with the relative height largest for the smallest amount of Cu and smallest for pure Cu. This suggests self-absorption—the Cu L_2-M_4 is strongly absorbed by the Cu L_3 edge (Kawai et al., 1993). Enhanced self-absorption is not an issue for K family lines as there is only one absorption edge and the K family X-rays must be less energetic than the edge. For the L shell, there are three absorption edges—L_1, L_2, and L_3. For Cu, they are located at 1.0961, 0.951, and 0.9311 keV, respectively. The Cu L_3-M_5 at 0.9295 keV is less energetic than any of the edges, but the Cu L_2-M_4, at 0.9494 keV, is

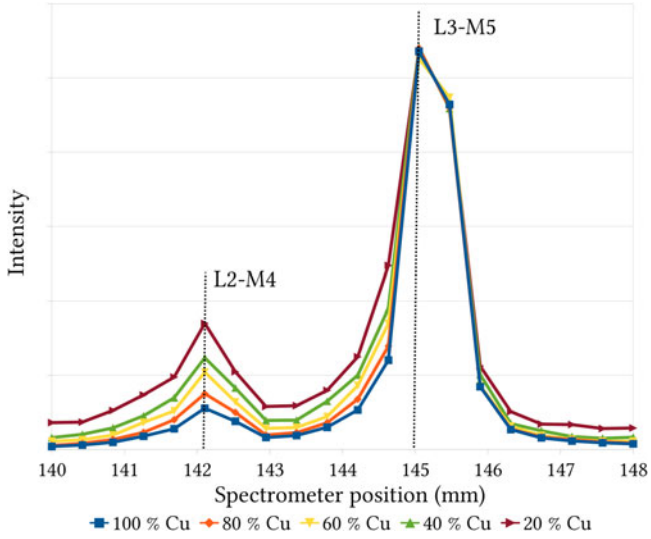

Figure 6. Comparing the Cu L3-M5 and Cu L2-M4 transition intensities as the relative amount of Cu in the material varies from 1.00 down to 0.20 via a wavelength scan. The intensities of the Cu L3-M5 are normalized to facilitate comparison.

between the L_2 and L_3 edges. The mass absorption coefficient for Cu is approximately 1,500 cm^2/g below the L_3 edge, approximately 9,000 cm^2/g between the L_2 and L_3 edges, and 12,000 cm^2/g above the L_2 edge. This means that the Cu L_2-M_4 is strongly absorbed by Cu while the Cu L_3-M_5 is much less strongly absorbed. The consequence is exhibited in Figure 6. When we attempt to account for absorption using a ZAF-type or $\varphi(\rho z)$-type quantitative correction algorithm, the correction for Cu L_2-M_4 shows entirely different behavior from the correction for Cu L_3-M_5. The absorption of Cu L_3-M_5 is dominated by absorption by Au, which increases as the proportion of Au increases. The absorption of Cu L_2-M_4 is dominated by the absorption by Cu and *decreases* as the proportion of Cu decreases. For the Cu L_3-M_5 transition in 80Au/20Cu, the absorption term is approximately 0.5, and for L_2-M_4 the absorption term is 2.0.

This observation has consequences not only for quantification of Cu by EDS, but also for quantification of any element in which a significant fraction of the total intensity falls between absorption edges. In general, quantifying EDS spectra require special care because families of lines are measured rather than narrow photon energy bands as with WDS.

To calculate the effective correction in the EDS case, all significant transitions need to be considered. The intensity measured in an EDS (I_x) experiment is the sum of the intensities from the individual transitions ($I_{x,tr}$), where x is either *std* or *unk*.

$$I_{unk} = \sum_{tr} I_{unk,\,tr} \quad \text{or} \quad I_{std} = \sum_{tr} I_{std,tr}. \tag{3}$$

Each transition has a quantitative correction factor for the unknown $[ZAF_{unk,\,tr}(C_{unk})]$ and the standard $[ZAF_{std,\,tr}(C_{std})]$, which are functions of the composition of the unknown (C_{unk}) and the standard (C_{std}).

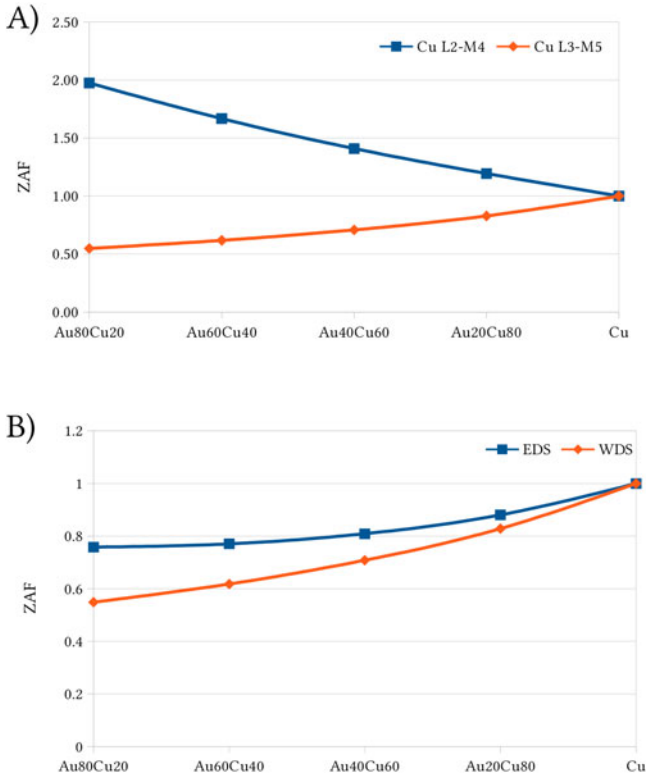

Figure 7. A: Compares the single transition correction factors for the Cu L2-M4 and Cu L3-M5 transitions as a function of the amount of Cu in a Au-Cu alloy. **B:** Compares the ZAF correction appropriate for WDS and EDS data for the Cu L3-M5 and the Cu L family, respectively.

$$I_{unk} = \sum_{tr} I_{std,\,tr} \left(\frac{C_{unk}}{C_{std}} \frac{ZAF_{unk,\,tr}(C_{unk})}{ZAF_{std,\,tr}(C_{std})} \right). \tag{4}$$

The intensity per transition for the standard can be expressed in terms of the total measured intensity for the standard and the weights of lines

$$I_{std,\,tr} = I_{std} \cdot w_{tr}, \tag{5}$$

where $\sum_{tr} w_{tr} = 1$.

Thus the measured intensity from the unknown can be expressed as

$$I_{unk} = \frac{C_{unk}}{C_{std}} I_{std} \left[\sum_{tr} w_{tr} \left(\frac{ZAF_{unk,\,tr}(C_{unk})}{ZAF_{std,\,tr}(C_{std})} \right) \right] \Big/ \left[\sum_{tr} w_{tr} \right], \tag{6}$$

where the term in square brackets is the effective quantitative correction for the EDS measurement.

The difference between the single line quantitative correction, and the correction derived in equation (6) for the Cu L-lines is shown in Figure 7. Quantifying the EDS data using the single line ZAF correction produces significant errors, but using equation (6) produces acceptable results.

Another consequence of equation (6) is that the Cu L line shape changes as a function of the mass fraction of Cu.

Table 5. The Experimental Configuration for the Ba-Ti Material Measurements.*

JXA-8500F—20 keV, 15 nA, 5 μm Probe									
Element	Standard	Line	Crystal	On (s)	High (s)	Low (s)	On Peak (mm)	High (mm)	Low (mm)
Ba	$BaCO_3$	L3-M5	PETJ	40	10	10	88.599	94.837	82.361
Ti	TiO_2	K-L3	PETJ	40	10	10	88.005	94.259	81.750
Ba	$BaCO_3$	L3-M5	LiF	40	10	10	193.033	194.988	188.961
Ti	TiO_2	K-L3	LiF	40	10	10	191.421	195.226	189.199
O	SiO_2	K-L3	LDE2	40	10	10	67.486	115.392	63.197
Si	SiO_2	K-L3	TAPJ	40	10	10	77.483	81.269	4.434
O	TiO_2	K-L3	LDE1	40	10	10	111.527	124.770	103.950
C	$BaCO_3$	K-L3	LDE2	40	10	10	125.188	142.488	110.488

*The measurements highlighted in gray are reported. OCR is the total output count rate for all four detectors. EDS: 60 s live time, ~12% dead time, 140 kcps OCR.

The consistency of the line shape is one of the fundamental assumptions in any standard/reference-based scheme for deconvolving spectral intensities. Fortunately, the influence of the change in line shape on the resulting *k*-ratios is minimal, except in the case of a particularly pernicious overlap. The consequences of the change in line shape can be observed in the residual derived from fitting 80Au/20Cu with a pure Cu reference. The residual is not as clean might be expected, but rather has a slight s-shape that is easily mistaken for an energy miscalibration.

The measured count rate must be corrected for the bremsstrahlung background. Only X-rays directly associated with a specific element—the characteristic X-rays—are of interest. Correcting for bremsstrahlung in WDS data typically involves making three measurements per characteristic line—a low background, an on-peak, and a high background. The background on-peak is then estimated by interpolating between the low background and the high background. The *k*-ratio is computed from the difference between the total count and the background count. With an SDD, all of the information necessary to perform bremsstrahlung correction is collected in a single measurement.

Ba-Ti Glasses

The experimental configuration for the Ba-Ti glasses is summarized in Table 5. The data were collected at 20 keV with a 15 nA probe current. The Ba, Ti, and O were measured on two different spectrometers. The lines highlighted in gray represent the measurements reported. The results are summarized in Figures 8 and 9.

The Ba-Ti glasses were selected to represent a difficult overlap situation, which would stress the capabilities of an energy dispersive spectrometer. The Ba L/Ti K overlap is often used to demonstrate the pitfalls of naive automatic peak ID algorithms and the importance of the residual spectrum as a diagnostic tool. Our materials ranged from Ba:Ti ratios of 2.9:1 to 24:1 by mass fraction.

Figures 8 and 9 provide two complementary presentations of the results. Figure 8 emphasizes the agreement between the SDD results and the WDS results. When plotted in this fashion, the figure emphasizes how extraordi-

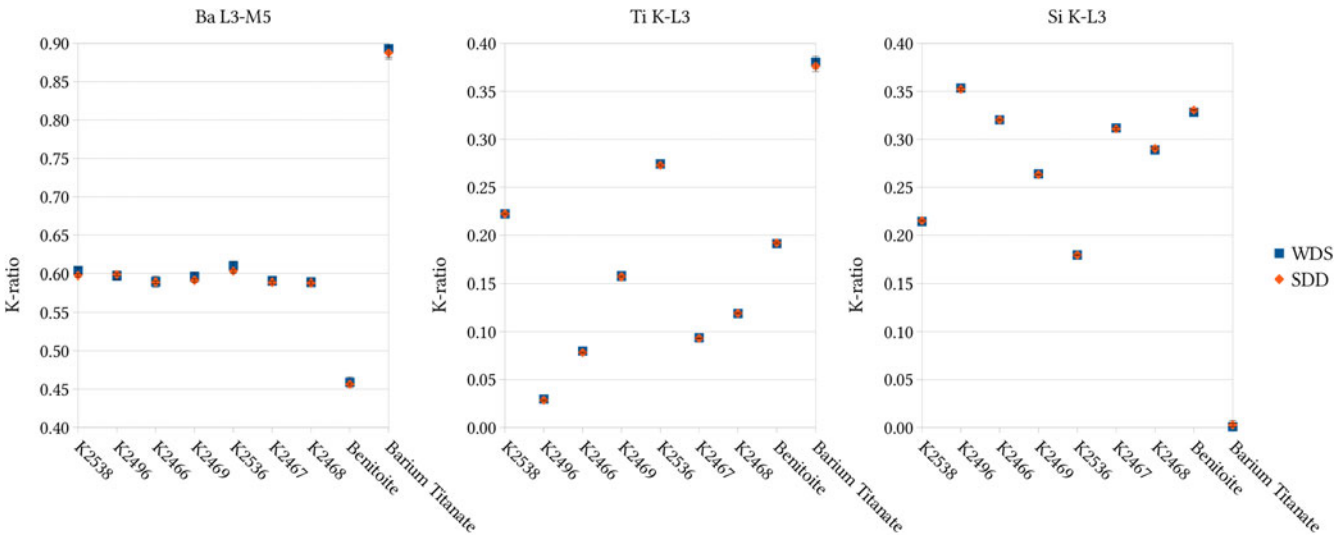

Figure 8. Comparing the *k*-ratios measured via SDD and WDS for nine different Ba-Ti containing materials.

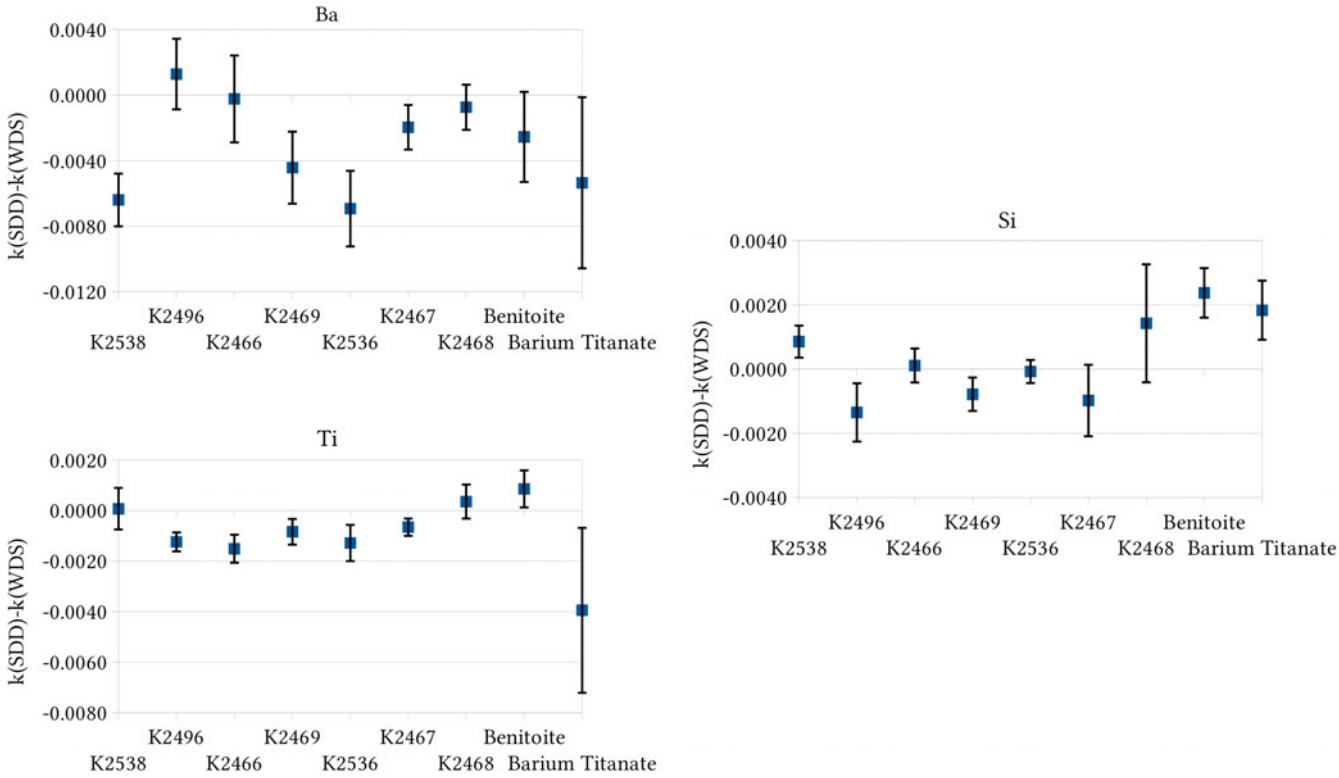

Figure 9. The difference of the *k*-ratio as measured with the SDD and the *k*-ratio as measured with WDS. The error bars represent 1σ variances of the eight distinct measurements of each material. The variances for the SDD and WDS measurements are added in quadrature.

narily well the magnitude of the SDD data matches the WDS data over a range of Ba, Ti, and Si mass fractions. The second presentation (Fig. 9) takes a more critical look at the variances. The agreement remains quite good. Ten of 27 (37%) data points are within 1σ and 21 (78%) are within 2σ. If the error was distributed normally, we would expect 68% of the values to fall within 1σ and 95% within 2σ. That the data exceed this suggests that there are some systematic differences between the SDD and WDS results. We are not able to determine whether these differences point to limitations of the SDD, limitations of WDS, or limitations of sample homogeneity.

Discussion

SDD and WDS are a contrast in strengths. A significant strength of the SDD is that a full spectrum is collected during each measurement. Because we have a full spectrum, we are much less likely to entirely miss the presence of an element. With high count spectra, elements down to the hundreds of ppm level need not be overlooked. The equivalent for WDS is taking a full wavelength scan—an operation that can take hours when sufficient count statistics to identify elements at the hundreds of ppm is required. Furthermore, the shape of the bremsstrahlung background on an SDD spectrum can be used as a diagnostic. The Duane-Hunt limit provides a means to diagnose sample charging or instrumental beam energy issues. The shape of the low energy background can indicate that the beam is in a pit, or if the X-rays are obstructed by surface contamination. In general, having access to the full spectrum provides more diagnostic information than WDS measurements. Of course, it is always possible to collect an X-ray spectrum along with WDS data and get the same benefits, but it is necessary to review the spectra. Since collecting an SDD spectrum at each point takes no more time than collecting only WDS data, it is easy to justify collecting both EDS and WDS for both standards and unknowns.

Collecting a full spectrum with each measurement is also a weakness. The total throughput of both SDD and WD spectrometers is limited. We may be interested in the intensities at a handful of characteristic line energies, but, with an SDD, one must invariably collect the full spectrum. With an SDD, you cannot avoid collecting both informative and less informative channel data, and the less informative data cost throughput without providing much benefit. On the other hand, with a wavelength spectrometer, the diffracting element filters out all but the energy of interest allowing you to apply the full throughput to informative data. This is particularly true for trace element analysis. The X-rays from a trace element may only represent a tiny fraction of the total X-rays in the spectrum. With a WD spectrometer, the entire throughput of the detector can be focused on collecting useful information. With an SDD, almost 100% of the throughput is commandeered by the bremsstrahlung or characteristic peaks of major constituents. Only a small

fraction remains to provide information about the trace element. The ability to filter out uninteresting X-rays is probably the most significant benefit of WDS—more so than even the high peak-to-background ratio.

While the spectral resolving power of the WDS contributes to enhance the discrete on-peak intensity and to decrease the diffuse background intensity, this advantage, although significant, is often overrated. If one performs a naive comparison between a three-point WDS measurement (on peak, high and low) and a three channel EDS measurement (on-peak, high and low), WDS readily wins. But this is not how EDS measurements are actually performed. A high quality EDS measurement involves fitting a reference spectrum to an unknown over a range of channels, which is typically on the order of 2 to 3 FWHM. The net result is uncertainties that are very competitive with equivalent wavelength measurements, except in trace element situations.

The SRM-479a sample represents a good example because the data were collected independently under optimal conditions for both SDD (12 nA) and WDS (100 nA). For Fe, the uncertainty on the Kα peak by SDD was 0.2%, and for the K-L_3 line by WDS was 0.3% for live times of 60 s and 40 s/10 s/10 s, respectively. The low uncertainty for the SDD can be attributed to the large number of counts. The peak region has 1.26×10^6 counts, and the background regions have 4.5×10^4 (low) and 3.6×10^4 (high).

Conclusion

In this article, we have demonstrated that a carefully performed and analyzed silicon drift EDS measurement can produce results that are as accurate and precise as carefully performed wavelength spectrometry results with equivalent or less time and effort. We hope this result will encourage instrument vendor's and technique users to invest in the design of a new generation of electron microprobes in which SDD and WDS are equal partners, and that software tools are developed to assist the user in optimizing the use of their system to produce the most accurate result with the minimal time and effort. By equal partners, we do not mean to suggest that SDD and WDS are equivalent or interchangeable. There are clearly measurements for which a WDS is better than an SDD, and vice versa. Determining the optimal detector for any particular *k*-ratio measurement can require deep insight into the measurement process and the performance characteristics of the detectors. Even an experienced analyst will be challenged to consistently make the optimal selection. However, thoughtfully written software can help, particularly if robust databases of detector performances are available.

With the availability of high-quality, high-throughput SDD, it is time to reconsider the role of energy dispersive spectrometry. While it remains true that there will always be a role for wavelength spectrometry performing trace analysis and for discerning minority elements in extreme overlap situations, our data suggest that in many cases the precision and accuracy of X-ray intensity measurements that can be achieved with an SDD is as good as a WDS in a fraction of the time and with a fraction of the effort. Moreover, with the SDD, all X-rays are measured in exactly the same angular space, while with multiple WDS each spectrometer represents a different absorption path. These advantages include some circumstances that might surprise people unfamiliar with high quality SDD analysis with standards. Even difficult overlaps can be handled with precision when there are sufficient counts in the standard and unknown spectra.

This is not to claim that the SDD should replace WDS in all circumstances. It is undeniable that the limits-of-detection are typically at least an order-of-magnitude better for WDS. To demonstrate the absence of an element by e-beam to the 10 ppm level, WDS remains the better choice. Furthermore, to accurately quantify elements at below the 1,000 ppm level, WDS is the best choice. But even in these circumstances, it is not necessary to collect all the data via WDS. Collecting major (greater than 0.10 mass fraction) and minor (less than major but greater than 0.01 mass fraction) elements via the SDD, and using WDS where it is needed will save time, require fewer spectrometers and eliminate blunders by providing redundant data and additional diagnostic information.

The systems we envision would look more like conventional microprobes than conventional SEMs, but with less emphasis on number of WDS detectors and more emphasis on EDS performance. The SDD design may be optimized differently to match the performance characteristics of the WDS detector. Small area SDD ($\sim$1 mm^2) might provide a better match between $[\Omega \cdot \epsilon]_{WDS}$ and $[\Omega \cdot \epsilon]_{SDD}$ and can produce higher ultimate throughput because the electronics can be tuned for a shorter worst-case rise time. Alternatively, a larger area SDD could be apertured, as is often done today with Si(Li) detectors, with slightly reduced maximum throughput. Many of the standard microprobe features (in-line probe current meter, planar *X*-*Y* stage, optical focusing microscope, high current stability electron guns) remain beneficial for high quality EDS measurements. We suspect that in the near future even dedicated WDS systems may have only one or two wavelength spectrometers. In this scenario, the software will have to automate both SDD and WDS acquisition and will have to use the best available algorithms for processing both data types. Furthermore, the software should assist the user in selecting the optimal accelerating voltage, probe current, acquisition times, and assignment of elements to detectors to perform the highest precision and accuracy measurements given the available tools and the user's precision and accuracy requirements.

It has long been true that the precision of EPMA measurements typically exceeds the accuracy of EPMA measurements. The precision that can be achieved by X-ray spectrometry is ultimately limited by count statistics. The accuracy is limited by the precision, but also by systematic errors embedded within the corrections, which are applied to compensate for the detailed physics of the measurement

process. The most common corrections for EPMA measurements compensate for electron stopping power, backscatter loss, X-ray absorption, and secondary fluorescence—the so-called $Z{\cdot}A{\cdot}F$ or $\varphi(\rho z)$ corrections. There are other corrections when the geometry does not meet the requirements for an ideal "bulk" sample, or when there are proximate materials that produce secondary fluorescence. Our ability to accurately model these corrections and our knowledge of accurate parameters (such as mean ionization potential, absorption cross sections, branching ratios) to input into these corrections ultimately limit our accuracy. Both the SDD and WDS can produce more than enough precision to not limit the measurement accuracy in almost all cases.

Making the most of the SDD requires standards-based analysis. It will require using equation (6) or an equivalent to handle the subtleties of quantitative correction for multiline peaks via $\varphi(\rho z)$ or $Z{\cdot}A{\cdot}F$. It will require automated data collection and reduction similar to what is available on modern microprobes.

Ultimately, it may be the prevalence of standardless analysis that has done the most damage to EDS's reputation (Newbury et al., 1995). Standardless analysis, while useful in certain limited circumstances, is not comparable in accuracy or precision with standards-based analysis. Standards-based analysis with EDS spectra is more time-consuming than standardless analysis, but significantly less time-consuming than standards-based analysis with WDS.

There are scenarios that are not adequately addressed in this article. We avoided low energy X-rays (below 1 keV in photon energy) in which absorption and bremsstrahlung make spectrum processing more difficult. We did not address some classic overlaps like Al/Br, S/Mo/Pb, or Ag/Th. We will report in a subsequent article additional investigations, which demonstrate that the SDD can handle these interferences better than we had initially expected.

References

Castaing, R. (1951). Application of electron probes to local chemical and crystallographic analysis. PhD Thesis, University of Paris [English translation by P. Duwez and D.B. Wittry, California Institute of Technology, 1955].

Chantler, C.T., Olsen, K., Dragoset, R.A., Chang, J., Kishore, A.R., Kotochigova, S.A. & Zucker, D.S. (2005). X-ray form factor, attenuation and scattering tables (version 2.1). Available at http://physics.nist.gov/ffast National Institute of Standards and Technology, Gaithersburg, MD. Originally published as Chantler, C.T. (2000). *J Phys Chem Ref Data* **29**(4), 597–1048 and Chantler, C.T. (1995). *J Phys Chem Ref Data* **24**, 71–643.

Egerton, R.F., Fiori, C.E., Hunt, J.A., Isaacson, M.S., Kirkland, E.J. & Zaluzec, N.J. (1991). EMSA/MAS standard file format for spectral data exchange. EMSA Bulletin 21 35-41. Available at ftp://www.amc.anl.gov/AMC-3/ANLSoftwareLibrary/2-EMMPDL/Xeds/EMMFF/emmff.doc.

Fiorini, C., Kemmer, J., Lechner, P., Kromer, K., Rohde, M. & Schulein, T. (1997). A new detection system for X-ray microanalysis based on a silicon drift detector with Peltier cooling. *Rev Sci Instrum* **68**(6), 2461–2465.

Gatti, E. & Rehak, P. (1984). Semiconductor drift chamber—An application of a novel charge transport scheme. *Nucl Instrum Methods* **225**, 608.

Jenkins, R., Manne, R., Robin, R. & Senemaud, C. (1991). Nomenclature, symbols, units and their usage in spectrochemical analysis—VIII. Nomenclature system for X-ray spectroscopy. *Pure Appl Chem* **63**(5), 735–746.

Kawai, J., Nakajima, K. & Gohshi, Y. (1993). Copper Lβ/Lα X-ray emission intensity ratio of copper compounds and alloys. *Spectrochim Acta* **48B**, 1281–1290.

Marinenko, R.B., Biancaniello, F., DeRobertis, L., Boyer, P.A. & Ruff, A.W. (1981). Preparation and characterization of an iron-chromium-nickel alloy for microanalysis: SRM 479a. Special Publication 260-70. Washington, DC: National Bureau of Standards.

Meinke, W.W. (1969*a*). Certificate of analysis, standard reference material 481, gold-silverwires for microprobe analysis. Washington, DC: National Bureau of Standards.

Meinke, W.W. (1969*b*). Certificate of analysis, standard reference material 482, gold-copper wires for microprobe analysis. Washington, DC: National Bureau of Standards.

Newbury, D., Swyt, C. & Myklebust, R. (1995). Standardless quantitative electron-probe microanalysis with energy dispersive X-ray spectrometry—Is it worth the risk. *Analyt Chem* **67**, 1866–1871.

Pouchou, J.L. & Pichoir, F. (1991). Quantitative analysis of homogeneous or stratified microvolumes applying the model "PAP." In *Electron Probe Microanalysis*, Heinrich, K.F.J. & Newbury, D.E. (Eds.). New York: Plenum.

Reed, S.J.B. & Ware, N.G. (1973). Quantitative electron microprobe analysis using a lithium drifted silicon detector. *X-Ray Spectrom* **2**, 69–74.

Ritchie, N.W.M. (2011). Standards-based quantification in DTSA-II—Part 1. *Microsc Today* **19**, 30–36.

Schamber, F.H. (1977). A modification of the linear least squares fitting method which provides continuum suppression. In *X-ray Fluorescence Analysis of Environmental Samples*, Dzubay, T. (Ed.). Ann Arbor, MI: Ann Arbor Science.

Statham, P. (1977). Pile-up rejection: Limitations and corrections for residual errors in energy dispersive spectrometers. *X-Ray Spectrom* **6**, 94–103.